



# On the design of Pt-Sn efficient catalyst for carbon monoxide and ethanol oxidation in acid and alkaline media

Rubén Rizo <sup>a</sup>, David Sebastián <sup>b</sup>, M<sup>a</sup> Jesús Lázaro <sup>b</sup>, Elena Pastor <sup>a,\*</sup>

<sup>a</sup> Departamento de Química, Instituto de Materiales y Nanotecnología, Universidad de La Laguna, Avda. Astrofísico Francisco Sánchez s/n, 38071, La Laguna, Santa Cruz de Tenerife, Spain

<sup>b</sup> Instituto de Carboquímica, CSIC, Miguel Luesma Castán 4, 50018, Zaragoza, Spain

## ARTICLE INFO

### Article history:

Received 6 April 2016

Received in revised form 13 June 2016

Accepted 14 July 2016

Available online 15 July 2016

### Keywords:

Ethanol electrooxidation

Pt-Sn electrocatalysts

Carbon nanofibers

Direct ethanol fuel cell

Alkaline media

## ABSTRACT

Pt-Sn catalysts supported on carbon, with different Pt-Sn atomic ratios (3:1, 1:1, 1:3), were prepared through the formic acid method (FAM) and supported on different carbon supports (nanofibers and carbon blacks) to study their behavior toward CO stripping and ethanol oxidation reaction (EOR). PtSn/C catalysts and supports were physicochemically characterized by XRD, EDX, XPS, TEM and TPD. Good particle dispersion onto the carbon support, similar particle sizes (around 4–5 nm) and the presence of tin oxides were observed in all cases. Sn insertion favored the development of the  $\text{Pt}_3\text{Sn}_1$  phase and the presence of higher oxidation states of both metals in the catalyst. Ethanol and adsorbed CO oxidation were studied at these materials both in acid and alkaline media, by linear sweep voltammetry and chronoamperometry. Higher EOR current densities were obtained with the increase in the amount of Sn in the samples, been those materials supported on CNF the ones with the best CO tolerance and catalytic activity toward this reaction. As expected, a great improvement of the EOR activity was found in alkaline media compared to sulfuric acid media, providing good expectative for these materials as catalysts for alkaline direct ethanol fuel cells.

© 2016 Elsevier B.V. All rights reserved.

## 1. Introduction

Nowadays, the importance of finding alternatives to petroleum is a worldwide concern, as oil extraction is costly and environmentally damaging, the burn of hydrocarbons releases carbon dioxide to the atmosphere, contributing to the global warming, and oil reserves are becoming scarce. Hydrogen used as an energy vector is the simplest and most efficient way to convert energy, but the required infrastructure is yet limited mainly due to the production costs and storage difficulties.

One good alternative to hydrogen is the use of small organic molecules containing hydrogen atoms (methanol, ethanol, formic acid, etc.) directly as a fuel in low temperature fuel cells. Ethanol presents several advantages: it can be obtained from the fermentation of biomass in large quantities (renewable), it is not toxic like methanol and has a high energy density [1,2]. The catalytic activity of Pt for the electrooxidation of hydrogen is very satisfactory but,

when electrooxidizing ethanol, the use of Pt as electrode entails some disadvantages. Among them, its low selectivity to the complete oxidation of ethanol to  $\text{CO}_2$  leads to low fuel efficiency and, thus, low power densities when compared for example to methanol even if the former has a higher theoretical energy density. Actually, the main ethanol electrooxidation products are acetic acid and acetaldehyde [3–5]. Pt needs high overpotentials to break the C–C bond from ethanol, forming some adsorbed C2 species in addition to CO-like intermediates which also need high overpotentials to be oxidized [6–8]. As a consequence, a fast Pt surface poisoning takes place, resulting in low ethanol oxidation reaction (EOR) currents.

Pt-Sn catalysts are currently considered the best binary formulation toward EOR. The properties of Pt-Sn/C catalysts have been extensively investigated for their application as anode materials for direct ethanol fuel cells (DEFCs) in the last years. Tsiakaras et al. studied the influence of Pt-Sn composition on the ethanol oxidation reaction, with metallic ratios ranging from  $\text{Pt}_1\text{Sn}_1$  to  $\text{Pt}_4\text{Sn}_1$  catalysts that were prepared by reduction with ethylene glycol [9]. They showed that the maximum power density obtained in a DEFC exhibits a “volcano-type” behavior with the Sn content in the catalyst. The apex of the volcano was attributed to an interplay of

\* Corresponding author.

E-mail addresses: [epastor@ull.edu.es](mailto:epastor@ull.edu.es), [elena.pastor.tejera@yahoo.es](mailto:elena.pastor.tejera@yahoo.es) (E. Pastor).

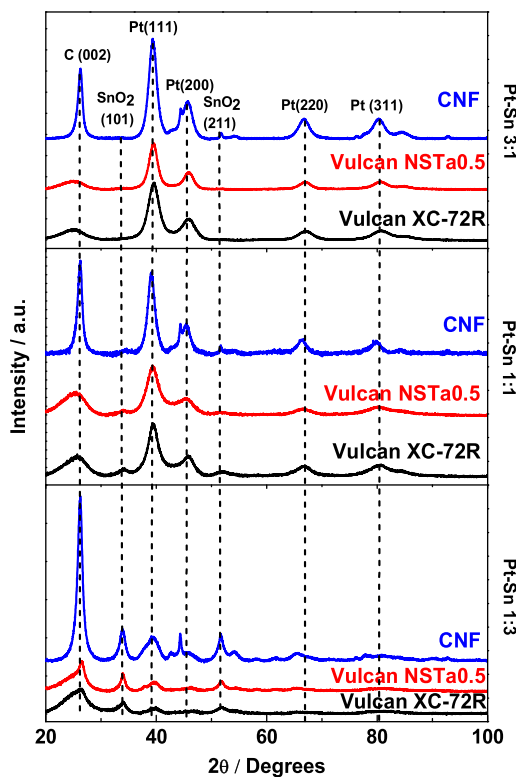


**Fig. 1.** X-ray diffractograms of samples.

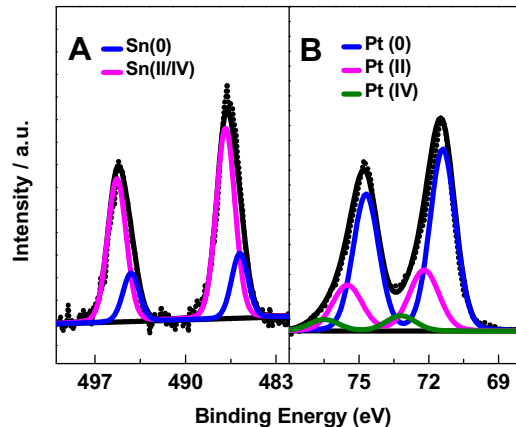


**Fig. 2.** (A) Sn 3d and (B) Pt 4f XPS spectra of Pt-Sn 3:1/Vulcan XC-72R.

enhanced activity with expanding lattice parameter and decreased conductivity with higher amounts of semiconducting tin oxide or decreased number of active sites of Pt partly covered by Sn [9]. The optimal Sn content for temperatures from 60 to 90 °C was found to be 30–40% [10], whereas a slightly higher optimum value of 50% [11,12] was reported for EOR at room temperature.

The higher electroactivity of this bimetallic formulation with respect to Pt has been explained by a bifunctional mechanism, i.e. Sn provides OH species at lower overpotentials than Pt, favoring the oxidation of intermediate species [13–15]. Other explanation is based on an electronic effect, which consists of the change of the electronic state of Pt atoms with the introduction of Sn, forcing the former to acquire different energy levels from the equilibrium. In this way, the weakening of Pt-CO bond is favored, which results in an easier removal of this adsorbate during the EOR [16]. However, the currents obtained in acid electrolytes by using Pt-Sn catalysts, although better than those for Pt, are still low.

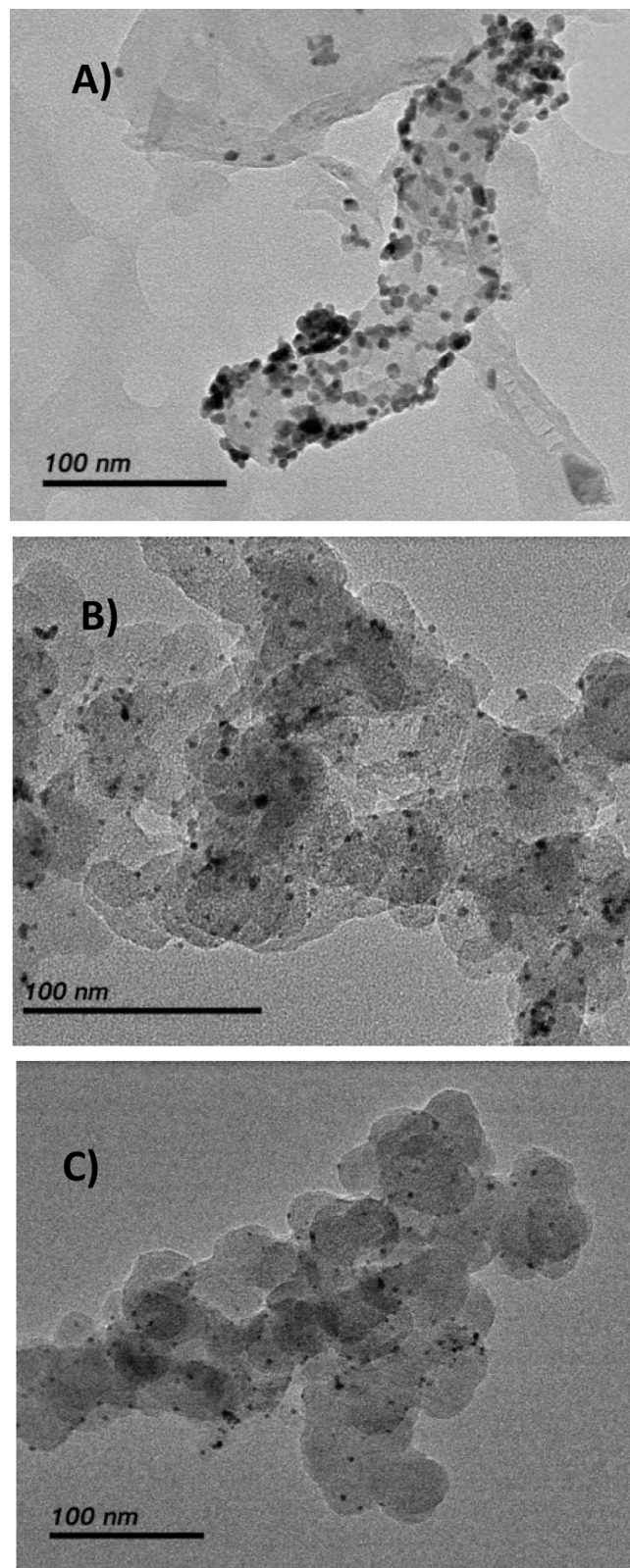


**Fig. 3.** TEM images of Pt-Sn 3:1 supported on: A) CNF B) Vulcan XC-72R C) Vulcan NSTa0.5.

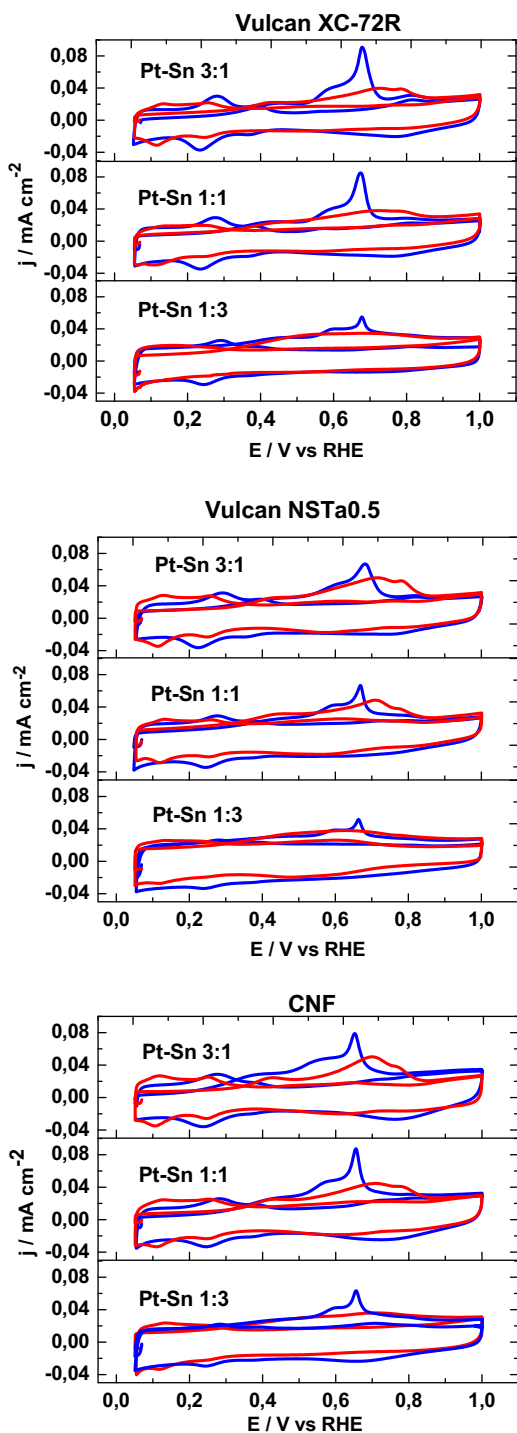


**Fig. 4.** CO-stripping voltammetry and CV in the base electrolyte for all catalysts recorded at 20 mV/s and 20 °C (0.5 M H<sub>2</sub>SO<sub>4</sub> (red solid line) and 0.1 M NaOH (blue dash-dot line)). Currents were normalized by the electrochemically active surface area obtained from CO-stripping measurements. (For interpretation of the references to colour in this figure legend, the reader is referred to the web version of this article.)

On the other hand, Pt based catalysts exhibit better activity and stability toward the EOR in alkaline media. This behavior has been attributed, at least in part, to the higher OH<sub>ad</sub> coverage at lower overpotentials [17]. Nevertheless, in alkaline media the electrolyte is prone to a progressive carbonation by the CO<sub>2</sub> generated in the EOR and from the atmosphere, which blocks the electrode porosity and reduces the catalytic efficiency. Some technologies

are being recently developed in order to solve this kind of problems, as the development of alkaline solid polymer membranes, which can greatly reduce the carbonation problems [18,19], or the employment of electrolyte recirculation systems which allows a continuous CO<sub>2</sub> removal [20].

Moreover, the support could also play a key role in the electroactivity of the catalyst toward the EOR. Carbon materials are generally used as support because they provide good electrical conductivity, good porosity where reactant molecules can easily transfer and react, high surface area for a suitable dispersion of metal particles and appropriate resistance to acid/alkaline environments [21–25]. The surface chemistry of carbon is also an important aspect to be considered for the design of highly active catalysts. It has been shown that the presence of oxygenated groups on the carbon surface improve the catalytic activity toward the EOR and favors the anchorage of metal nanoparticles on the carbon support [26,27]. In the present work, the functionalization of a carbon black (Vulcan XC-72R) with concentrated nitric and sulfuric acids was performed in order to create oxygenated groups on the surface [28].

Carbon nanofibers (CNFs) were also investigated as carbon support because they show interesting textural properties like low content in micropores (about 1% while Vulcan XC-72R has about 10%), where ethanol cannot transfer and react, and a graphitic structure which provides a high electrical and thermal conductivity as well as oxidation resistance [26,29,30].

Although CO and ethanol oxidation reactions on Pt-Sn/C catalysts have been extensively studied [9–16,31–33], no papers comparing the influence of the carbon support in different electrolytes and designing highly catalytically active Pt-Sn catalysts with atomic percentages of Sn higher than Pt have been published up to our knowledge.

In the present paper, Pt-Sn catalysts with different atomic ratios and supported on CNF, Vulcan and oxidized Vulcan, were synthesized and studied in acid and alkaline media in order to design an optimized material with the appropriate composition and carbon support to provide the highest catalytic activity toward EOR.

## 2. Experimental

### 2.1. Carbon support preparation

Oxidized Vulcan (labeled as Vulcan NSTa0.5) was prepared by oxidation of carbon black (Vulcan XC-72R from Cabot Co.) with concentrated nitric and sulfuric acids (Sigma Aldrich) at room temperature during 30 min under stirring conditions [28]. The oxidized carbon was then copiously washed with deionized water and dried at 110 °C overnight.

CNFs were synthesized by the catalytic decomposition of methane on a nickel-based catalyst (NiCuAl<sub>2</sub>O<sub>3</sub>) at 750 °C. The catalyst precursor (based on nickel-copper oxides) was firstly reduced in pure hydrogen at 550 °C for 1 h. The system was subsequently heated at 750 °C in an inert gas atmosphere and then pure methane was fed to the reactor (10 L g<sup>-1</sup> h<sup>-1</sup>) during 10 h. Further details can be found elsewhere [34].

### 2.2. Catalysts preparation

Pt-Sn catalysts supported on carbon were prepared by reduction of metal precursors with formic acid [35], by addition of a formic acid solution to the carbon support at 80 °C. Appropriate amounts of metal precursors (H<sub>2</sub>PtCl<sub>6</sub> and SnSO<sub>4</sub>, Sigma-Aldrich) were slowly added to the previous dispersion to obtain a metal loading of 20 wt.% in all cases.

### 2.3. Physicochemical characterization

Transmission electron microscopy (TEM), X-ray diffraction (XRD), energy-dispersive X-ray spectroscopy (EDX), X-ray photoelectron spectroscopy (XPS), temperature programmed desorption (TPD) and N<sub>2</sub> adsorption-desorption isotherms were employed for the physicochemical characterization of catalysts and/or carbonaceous supports.

N<sub>2</sub> adsorption-desorption isotherms of the carbon supports were measured at -196 °C using a Micromeritics ASAP 2020. The total surface area was calculated from BET (Brunauer, Emmett and Teller) equation and the total pore volume was determined using the single point method at P/P<sub>0</sub> = 0.99. Pore size distribution (PSD) curves were obtained from the analysis of the desorption branch of the N<sub>2</sub> isotherm using the BJH (Barrett, Joyner and Halenda) method.

The surface chemistry of the carbon materials was analyzed by TPD. The experiments were accomplished in a Micromeritics Pulse Chemisorb 2700 instrument, under a flow of helium and using a heating rate of 10 °C min<sup>-1</sup> from 150 °C up to 1050 °C. The amounts of CO and CO<sub>2</sub> desorbed from the samples were analyzed by gas chromatography.

Powder XRD patterns of Pt-Sn/C catalysts were recorded with a Panalytical X'Pert diffractometer using Cu-K $\alpha$  radiation. Scans were collected at 3° min<sup>-1</sup> for 2θ values between 20° and 100°.

The XPS analyses were performed with a VG-Microtech Multilab 3000 spectrometer equipped with a hemispherical electron analyser and a MgAl<sub>2</sub>X-ray source. The constant charging of the samples was corrected by referencing all energies to the C<sub>1s</sub> peak at 284.6 eV.

Pt-Sn atomic ratios and metal loading were determined by EDX, coupled to a scanning electron microscopy (SEM) LEO Mod. 440.

### 2.4. Electrochemical characterization

Electrochemical experiments were carried out in a conventional three-electrodes cell connected to an electrochemical analyzer (Autolab PGSTAT 302N). A high surface area carbon rod was used as counter electrode and a reversible hydrogen electrode (RHE) in the supporting electrolyte was employed as reference electrode. All potentials will be referred to the latter electrode.

The catalyst ink was prepared by ultrasonically dispersing 2 mg of the catalysts in 0.5 mL of ultrapure water (Millipore) and 15 μL of Nafion (5 wt%). An aliquot of the suspension was pipetted on the top of the working electrode consisting of a glassy carbon disk (7 mm), and dried at ambient temperature under N<sub>2</sub> atmosphere. The experiments were carried out in 0.1 M NaOH (99.99%, Merck) or 0.5 M H<sub>2</sub>SO<sub>4</sub> (Merck p.a.) aqueous solutions. First, the electrolyte was deaerated with pure Ar (99.998%, Air Liquide) and subsequently ethanol (Merck p.a.) was added for a 1 M concentration.

For the electrochemical characterization, cyclic voltammetry (CV) was employed, which consists of scanning the working electrode potential linearly versus time between two potential limits, recording the current generated. The CO stripping was performed bubbling the gas (99.997%, Air Liquide) for 10 min while polarizing the electrode at 0.07 V, then replacing non-adsorbed CO by bubbling Ar for 20 min, and subsequently scanning the potential up to 1 V at 20 mV s<sup>-1</sup>.

Current-time curves at constant potential (0.50 V) were recorded during 600 s to estimate the steady-state activity of the catalysts towards the EOR at a potential close to that at the anode side of a DEFC in the activation controlled region [36]. Current transients were carried out from 0.05 V, potential step where the

ethanol oxidation is negligible and then no adsorbed intermediates on Pt are present, to a potential of 0.50 V.

## 3. Results and discussion

### 3.1. Physicochemical characterization

The textural properties of the different carbon supports, analyzed by N<sub>2</sub>-physisorption measurements, are given in Table 1 [37]. As can be seen, only the total pore volume is slightly modified with the functionalization of the Vulcan support. CNFs show lower specific surface area (95 m<sup>2</sup> g<sup>-1</sup>) than carbon Vulcan (218 m<sup>2</sup> g<sup>-1</sup>), but approximately the 30% of the area of the later corresponds to micropores whereas for CNFs this contribution amounts only to 4%. This may lead to less mass transfer constraints in the catalytic layer based on CNFs support, facilitating ethanol molecules diffusion to catalytic sites.

The surface chemistry, in particular the amount of oxygen groups was evaluated by TPD experiments. The total amount of desorbed CO<sub>2</sub> and CO as well as the quantity of the different oxygenated groups is summarized in Table 2 [37]. It is shown that the chemical treatment of carbon Vulcan leads to a considerable increase in the presence of oxygenated groups on the carbon surface. Only small quantity of quinone groups can be seen in the untreated Vulcan XC-72R. After functionalization, a large amount of phenolic groups is created (1144 μmol g<sup>-1</sup>) along with some carboxylic acids, lactones and anhydrides (in decreasing order of quantity), whereas the amount of quinones diminishes to about the half. CNFs show a lower total contribution of oxygen groups (252 μmol g<sup>-1</sup>) compared to untreated Vulcan XC-72R. According to these results, the chemical functionalization treatment in acid results in the formation of oxygenated surface groups which can enhance the hydrophilicity of the support and may favor the metal particle anchoring, maintaining the textural properties of the untreated carbonaceous material.

XPS, XRD and EDX results are summarized in Table 3. Metal loading and Pt-Sn atomic ratios of the catalyst were determined by EDX analysis. The metal content and the Pt:Sn bulk atomic ratios (EDX) were similar to the nominal ones in all Pt-Sn/C catalysts, so there is no significant effect of carbon features on the metallic composition. Pt:Sn atomic ratios were also determined by XPS, showing similar values to those obtained by EDX, indicating that no significant metal segregation occurs at the surface.

X-ray diffractograms of Pt-Sn/C catalysts are given in Fig. 1. The typical face centered cubic (fcc) crystalline peaks of Pt are identified, namely the planes (111), (200), (220), (311) and (222). Apart from the Pt crystallographic structure signals, the graphitic carbon reflection plane (002) at 2θ = 24.5° and the tin oxide phase (SnO<sub>2</sub>) characteristic peaks at 2θ c.a. 34° and 52° are also identified, the latter for the Pt<sub>1</sub>Sn<sub>1</sub>/C and especially the Pt<sub>1</sub>Sn<sub>3</sub>/C samples. The CNF-supported catalysts present also two Ni fcc related reflections at 2θ values of about 44° and 52°, which come from the presence of Ni traces in the CNF.

The Pt lattice parameter was calculated from the Bragg equation for all Pt-Sn/C catalysts (Table 3). Regardless the support and metallic composition, all catalysts present higher lattice parameter values than that for pure platinum supported on carbon (3.92 Å), which may lead to an improvement of Pt-Sn interactions. In this sense, Antolini et al. found that the formic acid method allows the highest degree of Pt-Sn alloying compared to the most commonly employed synthesis methods for Pt-Sn/C catalysts [38]. It is important to note that Pt and Sn produce solid fcc alloys when the Sn content is lower than 25 at.% and hexagonal close packing (hcp) alloys when higher than 25 at.%. [8,39,40,41]. Since only fcc phases were observed at X-ray diffractograms, the amount of Sn alloyed to

**Table 1**

Textural properties of carbon supports.

Sample	$S_{\text{BET}}$ ( $\text{m}^2/\text{g}$ )	$V_{\text{Total}}$ ( $\text{m}^3/\text{g}$ )	$V_{\text{Micropore}}$ ( $\text{cm}^3/\text{g}$ )	$V_{\text{Mesopore}}$ ( $\text{cm}^3/\text{g}$ )	$S_{\text{Micropore}}$ ( $\text{m}^2/\text{g}$ )	$S_{\text{Mesopore}}$ ( $\text{m}^2/\text{g}$ )
XC-72R	218	0.41	0.03	0.38	65	153
XC-72R NSTa0.5	218	0.58	0.04	0.54	65	153
CNF	95.7	0.23	0.001	0.23	4.0	91.7

**Table 2** $\text{CO}_2$  and CO desorbed in TPD experiments from oxygen surface groups in the carbon materials.

Sample	$\text{CO}_2$ peak area ( $\mu\text{mol/g}$ )		CO peak area ( $\mu\text{mol/g}$ )			$\text{CO} + \text{CO}_2$ ( $\mu\text{mol/g}$ )	$\text{CO}/\text{CO}_2$
	Carboxyl	Lactone	Anhydride	Phenol	Carbonyl Quinone		
Vulcan XC-72R	0	0	0	0	317	317	–
Vulcan NSTa0.5	464	231	55	1144	140	2089	1.80
CNF	11	20	0	68	153	252	6.90

**Table 3**

Composition and structural characteristics obtained from XPS (\*), EDX (\*\*) and XRD (\*\*\*)�

Catalyst	Carbon support	Pt:Sn atomic ratio*	Pt:Sn atomic ratio**	Carbon content* (wt %)	Metal content** (wt %)	Crystallite size*** (nm)	Lattice parameter*** (Å)
Pt-Sn 3:1/C	Vulcan XC-72R	72:28	76:24	75	18	3.1	3.953
	Vulcan NSTa0.5	68:32	74:26	73	18.5	3.8	3.957
	CNF	70:30	73:27	57	19	4.1	3.968
Pt-Sn 1:1/C	Vulcan XC-72R	42:58	46:54	80	18	3.1	3.962
	Vulcan NSTa0.5	42:58	45:55	74	19	2.8	3.976
	CNF	45:54	46:54	61	18	5.1	3.988
Pt-Sn 1:3/C	Vulcan XC-72R	30:70	27:73	83	17.5	3.6	3.976
	Vulcan NSTa0.5	17:83	24:76	73	18.5	3.8	3.992
	CNF	20:80	23:77	54	18	3.2	3.993

Pt should be as high as 25 at%. Also the intensity of the peaks related to  $\text{SnO}_2$  species increases with the amount of Sn in the catalyst and the lattice parameter gets closer to  $4.001\text{\AA}$ , value which is ascribed to the pure intermetallic  $\text{Pt}_3\text{Sn}_1$  alloy (JPCDS 00-035-1360). These results indicate that both the degree of alloying between Pt and Sn and the relative amount of  $\text{SnO}_2$  phases increase in the order Pt-Sn 3:1 < Pt-Sn 1:1 < Pt-Sn 1:3, independently of the carbon support. In addition, CNF-supported Pt-Sn catalysts exhibit higher Pt lattice parameter than those supported on Vulcan XC-72R and Vulcan NSTa0.5, which reveals that the formation of  $\text{Pt}_3\text{Sn}_1$  phases is slightly favored when CNF is employed as support.

Pt crystallite sizes were calculated from the Scherrer equation and the broadening of the Pt (220) peak, resulting in similar values in the range 3–5 nm for all of them. It appears that there is not a clear effect of the support (functionalized or not) or the Pt:Sn composition on the Pt crystallite size. Finally, it is also noticeable that the relative intensity of the graphite-related peak (c.a.  $2\theta = 26^\circ$ ) is significantly higher for CNF compared to the carbon blacks (Vulcan XC-72R and Vulcan NSTa0.5), as expected from the high graphitization degree of CNF.

Fig. 2 shows the XPS of Pt 4f and Sn 4d spectra for the Pt-Sn 3:1 catalyst supported on Vulcan XC-72R, as a representative example. Pt 4f spectrum can be deconvoluted into three contributions ascribed to Pt (0), Pt (II) y Pt (IV) species, which appears at 71.4, 72.4 and 74.1 eV, respectively. On the other hand, the Sn 3d spectrum can be deconvoluted into two peaks attributed to Sn (0) at 485.8 eV and Sn (II/IV) at 487.4 eV. Discriminating between Sn (II) and Sn (IV) oxides is difficult because both species appears at very close binding energies. Table 4 summarizes the results regarding the deconvolution of Pt 4f and Sn 3d spectra for PtSn/C catalysts. It is observed that Sn is mostly in its oxidized state for all catalysts (61–97%). Pt and Sn tend to be in their oxidized form with the increase of Sn content, which suggests that Sn promotes the oxida-

tion of both metals in the material. Other interesting feature is that the weight percentage of carbon on the surface was lower than the nominal value (between 54 and 61%) for CNF supported catalysts, as can be seen in Table 3. This fact indicates that metal particles are more exposed on the surface of CNF-based catalysts compared to the other two carbon supports. An increase in the metal content on the surface may provide a higher density of catalytic active sites where the ethanol molecule can react, and consequently, a better performance of CNFs-based catalysts should be expected.

TEM images obtained for the Pt-Sn 3:1 catalysts supported on the different carbon supports employed are given in Fig. 3. The typical fibrous structure is envisaged for the CNF (Fig. 3a) whereas carbon black is formed by spheroidal agglomerates (Figs. 3b and c). A good distribution of metal particles on the supports was attained in all cases, with a regular particle size regardless the support, although some agglomerates were observed on the CNFs. This could be caused by the lower BET surface area of the nanofibers (Table 1).

### 3.2. Adsorbed CO electrooxidation (CO stripping)

First and second cyclic voltammograms (CVs) for the electrooxidation of CO adsorbed at  $0.07\text{ V}$  vs. RHE (CO stripping), are given in Fig. 4 for the three Pt-Sn compositions and the three supports (CNF, Vulcan XC-72R and Vulcan NSTa0.5). The current density ( $j$ ) has been normalized by the electroactive surface area estimated from the electrooxidation of a CO adsorbed monolayer. In a strict sense, this active surface area is assigned to Pt as only Pt atoms (and not Sn) adsorb CO. These CVs provide insights about the CO poisoning tolerance of synthesized materials, which is an important point to be considered for their use in direct alcohol fuel cell anodes, as CO is the main poisoning intermediate formed during alcohol oxidation. The onset for CO oxidation at Pt-Sn/C takes place at more negative potentials with respect to bare Pt catalysts in both acid and alka-

**Table 4**

Weight percentages of the different Pt and Sn species extracted from XPS experiment.

Catalyst	Carbon support	% Pt (IV)	% Pt (II)	% Pt	% Sn (II/IV)	% Sn
Pt-Sn 3:1/C	Vulcan XC-72R	9	19	72	77	23
	Vulcan NSTa0.5	2	17	81	65	35
	CNF	6	31	63	61	39
Pt-Sn 1:1/C	Vulcan XC-72R	10	20	70	83	17
	Vulcan NSTa0.5	14	24	62	74	26
	CNF	11	32	57	82	18
Pt-Sn 1:3/C	Vulcan XC-72R	12	31	57	89	11
	Vulcan NSTa0.5	16	29	55	95	5
	CNF	24	31	45	97	3

line electrolytes [42], indicating an increase in CO tolerance with the insertion of Sn. However, all materials developed an onset for CO oxidation at similar potentials (around 0.25 V), irrespective of carbon support or Pt:Sn ratio, which is in agreement with results from Lim and coworkers [43].

Three different contributions for CO oxidation are generally obtained in the stripping CVs for Pt-Sn catalyst in both electrolytes. This multiplicity of peaks can be explained by the presence of different active sites with diverse CO adsorption energy, the blocking effect by adsorbed species, as well as a slow CO surface diffusion towards reactive sites [44]. The first CO oxidation peak takes place at 0.45 V vs. RHE in alkaline and acidic media. It resembles a peak associated to Pt characterized by low coordinated sites or grain boundary [45]. The main oxidation peak is sharper in alkaline electrolyte than in sulfuric acid electrolyte, presumably due to the presence of sulfate anions in the latter which adsorbs on Pt active sites, making more difficult the mobility of CO on the surface in this medium. This main peak is located at more negative potentials on Pt-Sn/CNF (0.70 V vs. RHE in acid and 0.65 V vs. RHE in alkaline electrolyte) compared to Pt-Sn/Vulcan with and without functionalization (0.73 V vs. RHE in acid media and 0.68 V vs. RHE in alkaline electrolyte). CNF is thus the support that leads to a higher CO tolerance for Pt-Sn catalysts, while Vulcan functionalization doesn't improve significantly the activity of the catalysts toward CO oxidation.

The second cyclic voltammogram after CO stripping (CV in the base electrolytes), shows the hydrogen adsorption/desorption region typical for Pt catalysts in the 0.05–0.35 V potential range. A suppression of the currents in this region can be seen when the amount of Sn increases, which can be explained by the more facile adsorption of OH species with the presence of Sn or Sn oxides which hinders the hydrogen adsorption; the blockage of Pt adsorption sites; or a significant change in the electronic properties of Pt is produced by Sn insertion, as evidenced in XPS analyses [46]. The hydrogen adsorption/desorption peaks on sites with (110) and (100) orientations are more clearly pronounced in alkaline media (located at 0.25 and 0.35 V vs RHE, respectively) than in sulfuric acid (centered at 0.12 and 0.25 V vs RHE, respectively) [47], where sulfates anions are adsorbed on Pt blocking defect sites [48].

Furthermore, an anodic process takes place in the characteristic double layer region for Pt surfaces, which is related with catalyst surface oxidation promoted by Sn oxides [43]. On bare Pt catalysts supported on carbon Vulcan, surface oxidation takes place at potentials higher than 0.70 V vs. RHE [49], but after Sn insertion, the oxidation of the surface is shifted to more negative potentials (around 0.40 V vs. RHE), which suggests that the activation of H<sub>2</sub>O is promoted by Sn/SnO<sub>x</sub> species [50]. In alkaline media, however, hydrogen desorption is immediately followed by the oxidation of the surface because of the higher availability of OH in the electrolyte [51].

### 3.3. Ethanol electrooxidation

EOR was studied on Pt-Sn catalysts supported on Vulcan XC-72R, Vulcan NSTa0.5 and CNF by cyclic voltammetry in alkaline and acid electrolytes at room temperature. The working electrode was introduced into the solution at 0.05 V vs. RHE, where there is a negligible adsorption and electrooxidation of ethanol, and then a cyclic voltammogram was recorded up to 1.00 V vs. RHE at 0.02 V s<sup>-1</sup>. Fig. 5 shows the stable profiles (corresponding to the third cycle) in acid and alkaline electrolytes for all catalysts. Currents were again normalized by the electroactive surface area calculated from CO stripping experiments.

By comparing the currents and the onset potentials in the CVs for EOR, it is possible to establish the activity of the catalysts, being those which show lower onset potentials for the EOR and higher currents the most active ones. Hence, clearly, higher currents and more negative onset potentials (i.e. higher activities), are observed in alkaline medium than in sulfuric acid electrolyte. Two phenomena explain this increase in alkaline media: the absence of sulfate anions in the NaOH electrolyte, which adsorbs on Pt blocking some active sites [52]; and/or the higher coverage of adsorbed OH at low potentials in alkaline media, required for the removal of ethoxi residues, among others, during EOR [53]. It is also noticeable that the best electroactivity of the catalysts toward EOR is found for the catalysts with Pt:Sn atomic ratios 1:1, regardless the carbon support or the electrolyte, followed by Pt:Sn 1:3 based catalyst. The existence of an optimum Pt:Sn ratio implies that Sn species facilitate the ethanol oxidation at lower overpotentials than bare Pt, by means of bifunctional mechanism or electronic effect, as described in the introduction section; but ethanol adsorption and C–C bond dissociation requires Pt ensembles to accommodate the resulting dissociative-adsorption fragments during EOR [5–7,54,55]. The number of Pt active sites are limited when the Pt:Sn atomic ratio is 1:3. In this sense, Pt-Sn 1:1 appears to be the best formulation, in good agreement with the results found in Refs. [56] and [57].

Current transient curves at constant potential for EOR (1 M ethanol solutions) in acid and alkaline electrolytes for all catalysts are displayed in Fig. 6. The transients were carried out stepping from a potential where the ethanol oxidation is negligible ( $E_i = 0.05$  V vs RHE) to a potential of 0.50 V (typical potential for fuel cells in operation) during 600 s. The typical behavior for Pt-based electrodes was found in all cases, namely, a sharp current decay at short times finally attaining a stationary value. The current decrease rate depends on catalyst poisoning, most likely caused by CO<sub>ad</sub> and CH<sub>x,ad</sub> intermediates formed on the catalyst surface during the ethanol electrooxidation [58,6,7]. The catalyst with Pt:Sn atomic ratio equal to 1:1 was the one with the highest initial EOR currents, in agreement with the cyclic voltammetries. However, the stationary currents for Pt-Sn 1:1 and 1:3 catalysts were quite similar. Pt-Sn 1:3 catalysts are characterized by a quite low content of Pt, which is prone to poisoning by reaction intermediates. Moreover, Sn addition entails a crystalline structure effect leading to an increase of Pt<sub>3</sub>Sn<sub>1</sub> alloy content, as previously discussed, phase

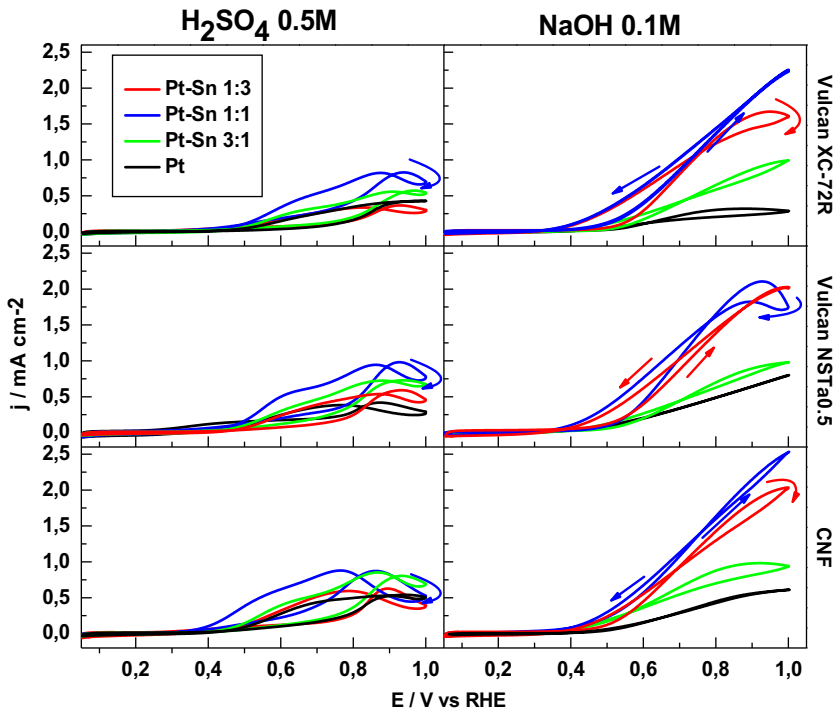


**Fig. 5.** Cyclic voltammograms for all catalysts recorded in 1 M ethanol at 20 mV/s and 20 °C in 0.5 M  $\text{H}_2\text{SO}_4$  (left) or 0.1 M  $\text{NaOH}$  (right). Currents were normalized by the electrochemically active surface area obtained from CO-strippling experiments.

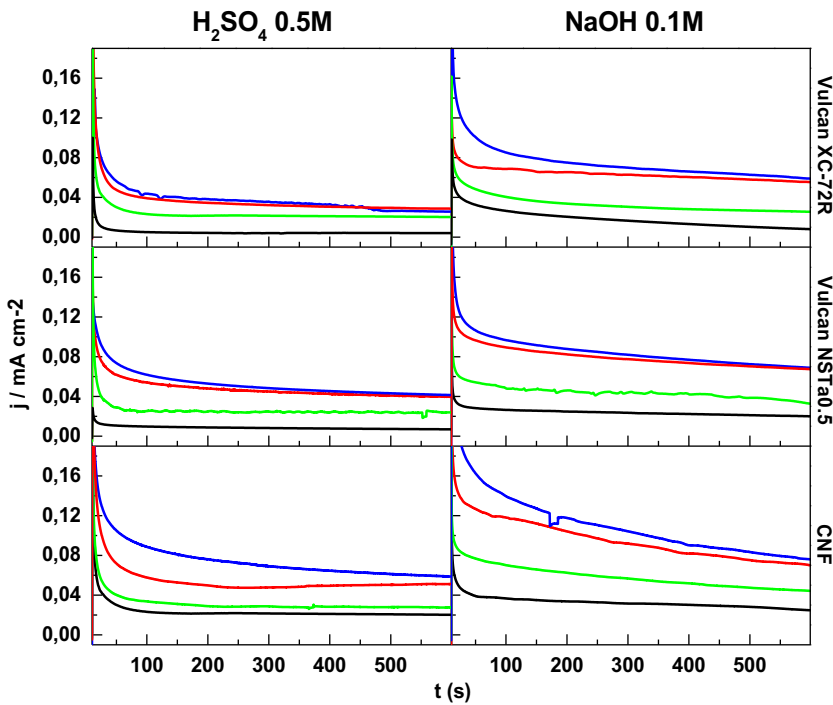


**Fig. 6.** Current-time curves for ethanol 1 M electrooxidation: comparison of Pt-(black solid line), Pt-Sn 3:1 (green solid line), Pt-Sn 1:1 (blue solid line) and Pt-Sn 1:3 (red solid line) recorded at 0.5 V in 0.5 M  $\text{H}_2\text{SO}_4$  (left) and 0.1 M  $\text{NaOH}$  (right) at 20 °C. Currents were normalized by the electrochemically active surface area obtained from CO-strippling experiments. (For interpretation of the references to colour in this figure legend, the reader is referred to the web version of this article.)

that has been ascribed in the literature as a promising catalyst for EOR [59]. Thus, although some works argue that the optimal atomic Sn content at room temperature is around 50% [11,12], this result suggests that catalysts with 75% of atomic Sn content show performances as high as those of catalysts with 50% Sn under steady-state conditions.

For an appropriate comparison of the effect of carbon supports, Fig. 7 shows the current-time curves of catalyst organized by the different Pt-Sn atomic ratios. Regardless the Pt-Sn composition or the electrolyte, the order of the activity for EOR decreases in this way: CNF > Vulcan NSTa0.5 > Vulcan XC-72R. The enhanced behavior of CNF-based Pt and  $\text{Pt}_x\text{Sn}_y$  catalysts can be attributed

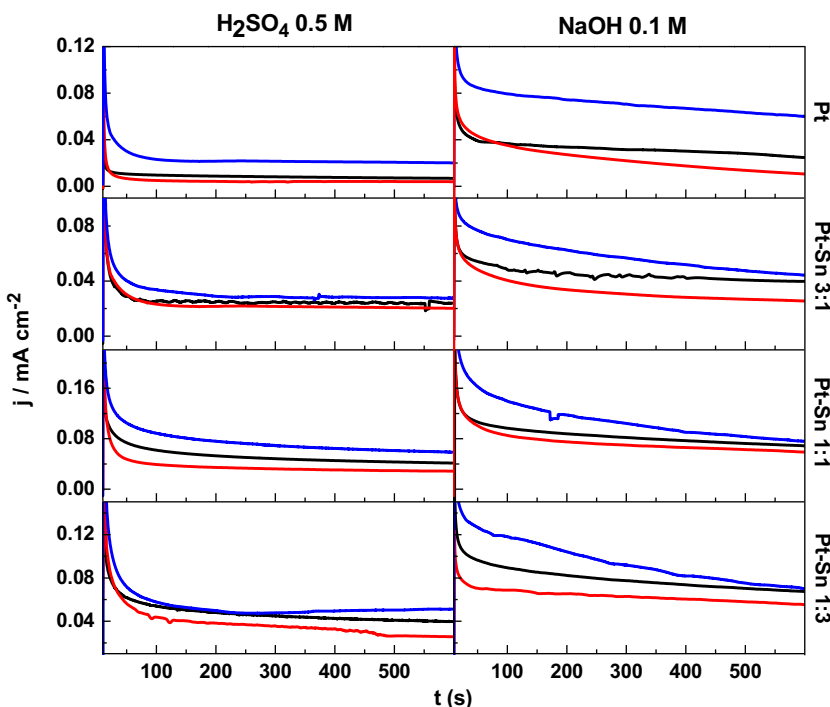


**Fig. 7.** Current-time curves for ethanol 1 M electrooxidation: comparison of CNF (blue solid line), Vulcan NSTa0.5 (black solid line) and Vulcan XC-72R (red solid line) recorded at 0.5 V in 0.5 M H<sub>2</sub>SO<sub>4</sub> (left) and 0.1 M NaOH (right) at 20 °C. Currents were normalized by the electrochemically active surface area obtained from CO-stripping experiments. (For interpretation of the references to colour in this figure legend, the reader is referred to the web version of this article.)

to several factors, including: CNF provides higher electrical conductivity than Vulcan XC-72R, due to its highly graphitic structure [25]; metal nanoparticles are more exposed on the surface of the catalyst, favoring the interaction between the metal onto the carbon and the ethanol molecule; the extent of the Pt<sub>3</sub>Sn<sub>1</sub> phase in the materials is slightly higher in CNF-supported catalysts, as evidenced by XRD; and the mesoporous area of CNFs is much higher than that of Vulcan, facilitating the mass transfer of the ethanol molecule and reaction products to/from the active sites of the catalysts. It seems also that oxygen surface groups promote the EOR, since Vulcan NSTa0.5 shows higher activity than Vulcan without functionalization.

In conclusion, it has been found that CNF is the support which develops the best behavior toward EOR and the Pt-Sn supported catalyst with atomic ratios 1:3 seems to be the best candidate in terms of high stationary currents at low Pt content.

#### 4. Conclusions

Formic acid reduction method (FAM) allowed the preparation of Pt-Sn catalysts supported on different carbon materials with metal loading and atomic ratios close to nominal values and a good dispersion. XPS analyses indicated that Sn is mostly in an oxidized state and promotes the oxidation of both metals in the catalysts. XRD results evidenced the presence of SnO<sub>2</sub> along with Pt, finding Pt crystallite sizes in the order of 3–5 nm. The relative quantity of Pt<sub>3</sub>Sn<sub>1</sub> crystallite phase in the materials increased with Sn content, having an important effect on the whole catalytic behavior towards CO and ethanol oxidation reactions.

The addition of Sn shifted the onset potential for adsorbed CO oxidation to more negative values with respect to bare Pt. Instead, it appeared that the atomic Pt:Sn ratio did not significantly influence the CO oxidation behavior, whereas the carbonaceous support affected the CO tolerance, being CNF the one with the lowest oxidation potential in both acid and alkaline electrolytes.

The chemical functionalization of Vulcan apparently did not significantly improve the tolerance toward CO oxidation.

Regarding the ethanol electrooxidation, the addition of Sn and, consequently, the content of Pt<sub>3</sub>Sn<sub>1</sub> crystallite phase, strongly improved the catalytic activity. Cyclic voltammograms showed lower activity for Pt-Sn 1:3 than for the Pt-Sn 1:1 catalysts, but similar stationary currents were found for both formulations in current transient curves, regardless the carbon support and electrolyte. This is an important result considering the low noble metal content of the Pt-Sn 1:3 material. In all cases, the activity of the catalysts toward EOR was higher in alkaline media than in sulfuric acid media.

An effect of carbon support on the Pt-Sn catalytic activity was also found, being CNF the one which showed the highest activities toward CO stripping and EOR. The oxidation treatment of Vulcan was also found to positively influence the EOR activity.

Summarizing, results in the present work provide an appropriate route to enhance the activity of Pt-Sn/C materials towards the ethanol electrooxidation from the point of view of catalyst formulation, by choosing appropriate support and metal composition.

#### Acknowledgements

This work has been supported by Fundación Canaria (project BIOGRAF) and the Ministry of Economy and Competitiveness (MINECO) through the projects CTQ2011-28913-C02-02 and ENE2014-52158-C2-2-R. R.R. is also indebted with the MINECO for the pre-doctoral grant.

#### References

- [1] C. Lamy, E.M. Belgsir, *J. Appl. Electrochem.* 31 (2001) 799.
- [2] J.-M. Léger, S. Rousseau, C. Coutanceau, F. Hahn, C. Lamy, *Electrochim. Acta* 50 (2005) 5118.
- [3] S.C. Zignani, V. Baglio, J.J. Linares, G. Monforte, E.R. Gonzalez, A.S. Aricò, *Electrochim. Acta* 70 (2012) 255.
- [4] Y. Paik, S.S. Kim, O.H. Han, *Electrochim. Commun.* 11 (2009) 302.

- [5] D.D. James, D.V. Bennett, G. Li, A. Ghuman, R.J. Helleur, P.G. Pickup, *Electrochim. Commun.* 11 (2009) 1877.
- [6] J. De Souza, S. Queiroz, *J. Phys. Chem. B* 106 (2002) 9825.
- [7] T. Iwasita, E. Pastor, *Electrochim. Acta* 39 (1994) 531.
- [8] T. Iwasita, E. Pastor, *Electrochim. Acta* 39 (1994) 547.
- [9] W.J. Zhou, S.Q. Song, W.Z. Li, Z.H. Zhou, G.Q. Sun, Q. Xin, S. Douvartzides, P. Tsakaras, *J. Power Sources* 140 (2005) 50.
- [10] P.E. Tsakaras, *J. Power Sources* 171 (2007) 107.
- [11] J.H. Kim, S.M. Choi, S.H. Nam, M.H. Seo, S.H. Choi, W.B. Kim, *App. Catal. B: Environ.* 82 (2008) 89.
- [12] E. Antolini, *J. Power Sources* 170 (2007) 1.
- [13] M. Arenz, C.A. Lucas, M.E. Gallagher, P.N. Ross, N.M. Markovic, *J. Am. Chem. Soc.* (2003) 2736.
- [14] T. Okanishi, T. Matsui, T. Takeuchi, R. Kikuchi, K. Eguchi, *Appl. Catal. A: Gen.* 298 (2006) 181.
- [15] K. Grass, H. Lintz, *J. Catal.* 152 (1997) 446.
- [16] E. Antolini, E.R. Gonzalez, *Electrochim. Acta* 55 (2010) 6485.
- [17] A.V. Tripković, K.D. Popović, *Electrochim. Acta* 47 (2002) 3707.
- [18] F. Bidault, D.J.L. Brett, P.H. Middleton, N.P. Brandon, *J. Power Sources* 187 (2009) 39.
- [19] E. Antolini, E.R. Gonzalez, *J. Power Sources* 195 (2010) 3431.
- [20] A.S. Hollinger, P.J.A. Kenis, *J. Power Sources* 240 (2013) 486.
- [21] J.C. Calderón, G. García, L. Calvillo, J.L. Rodríguez, M.J. Lázaro, E. Pastor, *Appl. Catal. B: Environ.* 165 (2015) 676.
- [22] C. Alegre, M.E. Gálvez, R. Moliner, V. Baglio, A.S. Aricò, M.J. Lázaro, *Appl. Catal. B: Environ.* 147 (2014) 947.
- [23] V. Celorrio, J. Flórez-Montaña, R. Moliner, E. Pastor, M.J. Lázaro, *Int. J. Hydrogen Energy* 39 (2014) 5371.
- [24] M. Wang, F. Xu, J. Xie, *Electrochim. Acta* 63 (2012) 295.
- [25] C.W.B. Bezerra, L. Zhang, H. Liu, K. Lee, A.L.B. Marques, E.P. Marques, H. Wang, J. Zhang, *J. Power Sources* 173 (2007) 891.
- [26] D. Sebastián, I. Suelves, R. Moliner, M.J. Lázaro, *Carbon N. Y.* 48 (2010) 4421.
- [27] C. Alegre, M.E. Gálvez, E. Baquedano, E. Pastor, R. Moliner, M.J. Lázaro, *Int. J. Hydrogen Energy* 37 (2012) 7180.
- [28] L. Calvillo, V. Celorrio, R. Moliner, M.J. Lázaro, *Mater. Chem. Phys.* 127 (2011) 335.
- [29] D. Sebastián, J.C. Calderón, J.A. González-Expósito, E. Pastor, M.V. Martínez-Huerta, I. Suelves, R. Moliner, M.J. Lázaro, *Int. J. Hydrogen Energy* 35 (2010) 9934.
- [30] D. Sebastián, I. Suelves, E. Pastor, R. Moliner, M.J. Lázaro, *Appl. Catal. B: Environ.* 132–133 (2013) 13.
- [31] M.Z.F. Kamarudin, S.K. Kamarudin, M.S. Masdar, W.R.W. Daud, *Int. J. Hydrogen Energy* 38 (2013) 9438.
- [32] A. Brouzgou, S.Q. Song, P. Tsakaras, *Appl. Catal. B: Environ.* 127 (2012) 371.
- [33] A. Brouzgou, A. Podias, P. Tsakaras, *J. Appl. Electrochem.* 43 (2013) 119.
- [34] D. Sebastián, I. Suelves, M.J. Lázaro, R. Moliner, *J. Power Sources* 192 (2009) 51.
- [35] E.R. Gonzalez, T.E.A., A.L.N. Pinheiro, J. Perez, INPI-SP, vol. 00321 Brazil, 1997.
- [36] S.C. Zignani, V. Baglio, D. Sebastián, S. Siracusano, A.S. Aricò, *Electrochim. Acta* 191 (2016) 183.
- [37] J. Asgardi, J.C. Calderón, F. Alcaide, A. Querejeta, L. Calvillo, M.J. Lázaro, G. García, E. Pastor, *Appl. Catal. B: Environ.* 168–169 (2015) 33.
- [38] E. Antolini, E.R. Gonzalez, *Catal. Today* 160 (2011) 28.
- [39] C. Lamy, S. Rousseau, E. Belgsir, C. Coutanceau, J.-M. Léger, *Electrochim. Acta* 49 (2004) 3901.
- [40] Á. Lerhun, F. Delime, C. Lamy, A. Lima, C. Coutanceau, J. Le, *J. Power Sources* 105 (2002) 283.
- [41] W. Zhou, B. Zhou, W. Li, Z. Zhou, S. Song, G. Sun, Q. Xin, S. Douvartzides, M. Goula, P. Tsakaras, *J. Power Sources* 126 (2004) 16.
- [42] A.C. Xps, R.D.E. Study, 145 (1998) 925.
- [43] D.-H. Lim, D.-H. Choi, W.-D. Lee, H.-I. Lee, *Appl. Catal. B: Environ.* 89 (2009) 484.
- [44] G. García, M.T.M. Koper, *ChemPhysChem* 12 (2011) 2064.
- [45] O. Guillén-Villafuerte, G. García, A. Orive, B. Anula, A. Creus, E. Pastor, *Electrocatalysis* 2 (2011) 231.
- [46] F.B. Passos, M. Schmal, M.A. Vannice, *J. Catal.* 117 (1996) 106.
- [47] Francisco J. Vidal-Iglesias, Rosa M. Arán-Ais, José Solla-Gullón, Enrique Herrero, Juan M. Feliu, *ACS Catal.* 2 (2012) 901.
- [48] A.V. Tripković, K.D. Popović, B.N. Grgur, B. Blizanac, P.N. Ross, N.M. Marković, *Electrochim. Acta* 47 (2002) (3707).
- [49] O. Guillén-Villafuerte, G. García, J.L. Rodríguez, E. Pastor, R. Guil-López, E. Nieto, J.L.G. Ferro, *Int. J. Hydrogen Energy* 38 (2013) 7811.
- [50] J.O.M. Bockris, S.U.M. Khan, *Surface Electrochemistry: A Molecular Level Approach*, Plenum Press, New York, 1993, pp. 4.
- [51] L. Ma, D. Chu, R. Chen, *Int. J. Hydrogen Energy* 37 (2012) 11185.
- [52] D.V. Tripkovic, D. Strmcnik, D. Van Der Vliet, V. Stamenkovic, N.M. Markovic, *Faraday Discuss.* 140 (2009) 25.
- [53] L. Jiang, A. Hsu, D. Chu, R. Chen, *Int. J. Hydrogen Energy* 35 (2010) 365.
- [54] O. Guillén-Villafuerte, G. García, C. Arévalo, J.L. Rodríguez, E. Pastor, *Electrochim. Commun.* 63 (2015) 48.
- [55] J. Flórez-Montaña, G. García, O. Guillén-Villafuerte, J.L. Rodríguez, G.A. Planes, E. Pastor, *Electrochim. Acta* 209 (2016) 121.
- [56] W. Zhou, *Solid State Ionics* 175 (2004) 797.
- [57] E.V. Spinacé, M. Linardi, A.O. Neto, *Electrochim. Commun.* 7 (2005) 365.
- [58] J. Ribeiro, D.M. dos Anjos, K.B. Kokoh, C. Coutanceau, J.-M. Léger, P. Olivi, A.R. de Andrade, G. Tremiliosi-Filho, *Electrochim. Acta* 52 (2007) 6997.
- [59] R.F.B. De Souza, L.S. Parreira, D.C. Rascio, J.C.M. Silva, E. Teixeira-Neto, M.L. Calegaro, E.V. Spinace, A.O. Neto, M.C. Santos, *J. Power Sources* 195 (2010) 1589.